ACS APPLIED MATERIALS & INTERFACES

www.acsami.org Research Article

Promoting Large-Area Slot-Die-Coated Perovskite Solar Cell Performance and Reproducibility by Acid-Based Sulfono-γ-AApeptide

Seid Yimer Abate,[⊥] Ziqi Yang,[⊥] Surabhi Jha, Jada Emodogo, Guorong Ma, Zhongliang Ouyang, Shafi Muhammad, Nihar Pradhan, Xiaodan Gu, Derek Patton, Dawen Li, Jianfeng Cai,* and Qilin Dai*

Cite This: https://doi.org/10.1021/acsami.3c02571 Read Online

ACCESS | Metrics & More | Article Recommendations | Supporting Information

ABSTRACT: Homogeneous and pinhole-free large-area perovskite films are required to realize the commercialization of perovskite modules and panels. Various large-area perovskite coatings were developed; however, at their film coating and drying stages, many defects were formed on the perovskite surface. Consequently, not only the devices lost substantial performance but also their long-term stability deteriorated. Here, we fabricated a compact and uniform large-area $MAPbI_3$-perovskite film by a slot-die coater at room temperature (T) and at high relative humidity (RH) up to 40%. The control slot-die-coated perovskite solar cell (PSC) produced 1.082 V open-circuit voltage (V_{oc}), 24.09 mA cm^{-2} short current density (J_{sc}), 71.13% fill factor (FF), and a maximum power conversion efficiency (PCE) of 18.54%. We systematically employed a multi-functional artificial amino acid (F-LYS-S) to modify the perovskite defects. Such amino acids are more inclined to bind and adhere to the perovskite defects. The amino, carbonyl, and carboxy functional groups of F-LYS-S interacted with $MAPbI_3$ through Lewis acid−base interaction and modified iodine vacancies significantly. Fourier transform infrared spectroscopy revealed that the C═O group of F-LYS-S interacted with the uncoordinated Pb^{2+} ions, and X-ray photoelectron spectroscopy revealed that the lone pair of $-NH_2$ coordinated with the uncoordinated Pb^{2+} and consequently modified the I^- vacancies remarkably. As a result, the F-LYS-S-modified device demonstrated more than three-fold charge recombination resistance, which is one of the primary requirements to fabricate high-performance PSCs. Therefore, the device fabricated employing F-LYS-S demonstrated remarkable PCE of 21.08% with superior photovoltaic parameters of 1.104 V V_{oc}, 24.80 mA cm^{-2} J_{sc}, and 77.00%. FF. Concurrently, the long-term stability of the PSCs was improved by the F-LYS-S post-treatment, where the modified device retained *ca.* 89.6% of its initial efficiency after storing for 720 h in air ($T \sim 27$ °C and RH ~ 50−60%).

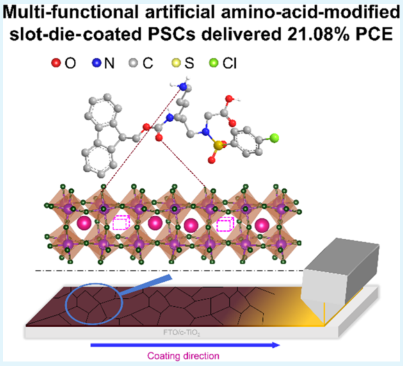

KEYWORDS: *slot-die coating, sulfono-γ-AApeptide, large-area perovskite layer, defects, perovskite solar cells*

■ INTRODUCTION

The laboratory-scale small-aperture area perovskite solar cells (PSCs) exhibited remarkably high certified performance above 25% power conversion efficiency (PCE).[1] However, the large-area perovskite device efficiency and lab-to-lab reproducibility are still lagging compared to small-area devices. In general, even for small-area devices, there is a substantial performance gap between the theoretically predicted and the current record PSCs. The Shockley−Queisser (SQ) limit predicted that the performance of PSCs with a band gap of 1.6 eV could deliver a maximum PCE of 30.14% with short current density (J_{sc}) = 25.47 mA cm^{-2}, open-circuit voltage (V_{oc}) = 1.309 V, and fill factor (FF) = 90.5%.[2] However, until now, the record perovskite device demonstrated a PCE of 25.7 ± 0.8% with J_{sc} = 25.80 mA cm^{-2}, V_{oc} = 1.179 V, and FF = 84.6%.[3] As is seen from the values, the V_{oc} and FF are critical to improving the device performance to approach the SQ PCE limit, and the J_{sc} has already reached the limit. One of the main causes for FF and V_{oc} loss is the concentration of defects in the polycrystalline perovskite, which cause severe non-radiative recombination in the surface and/or bulk of the perovskite.[2] Moreover, the interface between perovskite/hole transport layer (HTL) and perovskite/electron transport layer (ETL) also resulted in parasitic resistance, which limits the V_{oc} and FF.[3] PSCs prepared by the spin-coating method produced the champion performance; however, the technique is limited to small areas and not efficient to produce large films. The performance of spin-coated films deteriorated with increasing area; as a result, this technique will not be directly employed to prepare large-

Received: February 22, 2023
Accepted: May 5, 2023

ACS Publications

https://doi.org/10.1021/acsami.3c02571
ACS Appl. Mater. Interfaces XXXX, XXX, XXX−XXX

area modules and panels.[4] Higuchi fabricated a 354 cm^2 aperture area $MAPbI_3$-based sub-module by spin-coating; however, the champion performance of the devices is limited to 12.6% PCE.[5] Consequently, alternative large-area perovskite fabrication techniques, including thermal deposition, spray-coating, ink-jet printing, bar-coating, blade-coating, solution shearing, and slot-die coating, have been developed, aiming to fabricate homogeneous and pinhole-free large-area perovskite films to realize the highly efficient perovskite module.[6−11] Among all the large-area coatings, the slot-die technique provides accurate control over the film coating parameters, leading to the production of homogeneous and uniform large-area perovskite films. This is an important factor in fabricating commercial large-area perovskite films with uniform thickness and optoelectrical properties. The slot-die coater is a metered instrument that has precise control over the coating speed, coating gap, coating temperature, and coating flowrate; particularly, the last parameter is present only in the slot-die coater among the other large-area perovskite solution-processing techniques.[12] As a result, the slot-die coating is much more reproducible, and the optimized coating processes could be directly integrated into the industrial and commercial setups, including the roll-to-roll (to fabricate perovskite on flexible substrates) and sheet-to-sheet (to fabricate perovskite on rigid substrates) processes.[13]

Recently, various perovskite precursor solutions were slot-die-coated, aiming to fabricate large-area perovskite films and demonstrating promising PCE. Whitaker *et al.* achieved 18% PCE by slot-die $MAPbI_3$ precursor [prepared by dimethylformamide/*N*-methyl pyrrolidone (8:9 v/v) solvents] on ITO/SnO_2.[12] Moreover, the sequentially slot-die-coated $Cs_{0.05}MA_{0.4}FA_{0.55}Pb(I_{0.96}Br_{0.04})_3$ produced 19% PCE,[14] and the MAI-free slot-die-coated $Cs_{0.16}FA_{0.84}Pb(I_{0.88}Br_{0.12})_3$ demonstrated 18% PCE.[15] The uniformity and homogeneity of slot-die-prepared perovskite layer are influenced by a combination of various processing conditions such as precursor properties (precursor viscosity and meniscus stability), coating parameters (coating gap, coating flow rate, coating speed, and coating temperature), substrate surface properties (surface tension and surface energy), and post-processes (post-annealing temperature).[11] Therefore, the perovskite slot-die coating process required precise optimization of such a large number of processing conditions to achieve homogeneous morphology and uniform optoelectronic properties over a large area. The perovskite slot-die coating process favors high surface energy and a smooth underlayer substrate surface for uniform coating to achieve homogeneous film morphology and uniform thickness over a large area.

In general, the perovskite films prepared by the slot-die coating produced polycrystalline films like the spin-coating perovskite layers; consequently, the films contained a high density of defects, including antisites (such as PbI_3^-), cation vacancies (such as MA^+), halide vacancies (such as I^-), uncoordinated Pb^{2+}, uncoordinated I^-, and Pb clusters, or a combination of defects.[11,16] Such defects are the main source of non-radiative recombination and negatively influences the charge transport and extraction in the PSCs, which limits the device performance.[17] These defects also aggravated the perovskite degradation and influenced the device long-term stability. The uncoordinated ions in the defective perovskite layer could migrate through the grain boundaries and cause severe device hysteresis. Therefore, it is required to design efficient passivation molecules to eliminate such defects for superior PCE and device stability.[11,18] In general, there are four approaches to passivate the perovskite surface, grain boundary, and electronic defects.[11] These are (1) modifying the perovskite bulk defects by additive engineering,[19] (2) post-surface passivation of the perovskite film,[20] (3) pre-surface passivation (before perovskite layer deposits),[21] and (4) a combination of pre-surface passivation and post-surface passivation, in short, dual passivation, to modify both interfaces. Correspondingly, various passivation molecules were developed and demonstrated significant improvements in the PCE and stability by modified halide vacancies,[22−25] cation vacancies,[23,26,27] and both cation and halide vacancies from the perovskite layer.[17,18,28−32] Passivation molecules, including polymers, small molecules, and halide replacements with different functional groups such as −C═O, −N, −S, −S−N, −I, and −Cl were employed to modify the perovskite defects.[16] These molecules with a specified functional group have coordinated with the uncoordinated Pb^{2+} of perovskite and modified the halide vacancies.[16] Recently, poly-BCP was used to modify both the SnO_2 electron-transport layer and perovskite defects; as a result, a maximum PCE of 24.43% was achieved.[33] Ji *et al.* reported difunctionalized BTZI-TPA-passivated perovskite with a champion PCE of 24.06%, where the molecule formed a stronger interaction with uncoordinated Pb^{2+} on the perovskite surface; consequently, the non-radiative recombination of the perovskite was significantly reduced.[34] −COO−, −C(═NH)NH_2 functional group-containing (α-methylguanido)acetic acid-passivated $(FAPbI_3)_{0.95}(MAPbBr_3)_{0.05}$ produced a maximum PCE of 22.6%.[35] Post-treatment of $Cs_{0.03}(FA_{0.90}MA_{0.10})_{0.97}PbI_3$ by 2D oleylammonium iodide-based passivation demonstrated more than 24% PCE.[36] Additionally, 3-(trifluoromethyl)phenethylamine hydroiodide (CF_3PEAI) was employed for post-surface passivation, where it coordinated with the uncoordinated Pb^{2+} and modified defects.[37] Furthermore, some amino acid molecules with amino, carboxyl, and carbonyl groups showed effective coordination with the perovskite and modified defects significantly.[38−42]

Unlike the small-area cells, there are only a few reports on the passivation of slot-die-coated perovskite layers.[21,43−46] Potassium thiocyanate (KSCN) was added to improve the morphology of slot-die-coated $MAPbI_3$, and as a result, large perovskite grains were produced.[19] The 12% dimethyl sulfoxide-added $MAPbI_3$ precursor produced a homogeneous morphology of the slot-die-prepared $MAPbI_3$ layer.[47] Likewise, with respect to morphology improvement on the slot-die-coated perovskite film, Yang *et al.* added diphenyl sulfoxide additive to slow down the crystallization of $FA_{0.83}Cs_{0.17}PbI_{2.83}Br_{0.17}$.[48] All the above additives were directly added to the perovskite bulk precursor, and they were slot-die-coated together as a perovskite ink; as a result, the additives could change the precursor viscosity and precursor stability and could directly participate in the perovskite crystallization/growth process; consequently, it is hard to understand the sole advantage of the additives on the defect passivation.

Here, we report the post-surface passivation of the slot-die-coated $MAPbI_3$ layer with a newly synthesized artificial amino acid, F-LYS-S, a sulfonoyl-γ-AApeptide with multiple interaction sites to modify the perovskite defects.[49] F-LYS-S has −COOH, −C═O, −NH, and $-NH_2$, which can form interactions with perovskite defects. To remove the influence of ETL on the morphology/reproducibility of the slot-die-coated perovskite, we developed a large-area c-TiO_2 film using

Scheme 1. Illustration of Fabrication of the Large-Area Perovskite Layer by a Slot-Die Coater on Large-Area Water-Bath-Prepared c-TiO_2[11] and Passivation of Prepared Perovskite by Multi-functional Artificial Amino-Acid of F-LYS-S

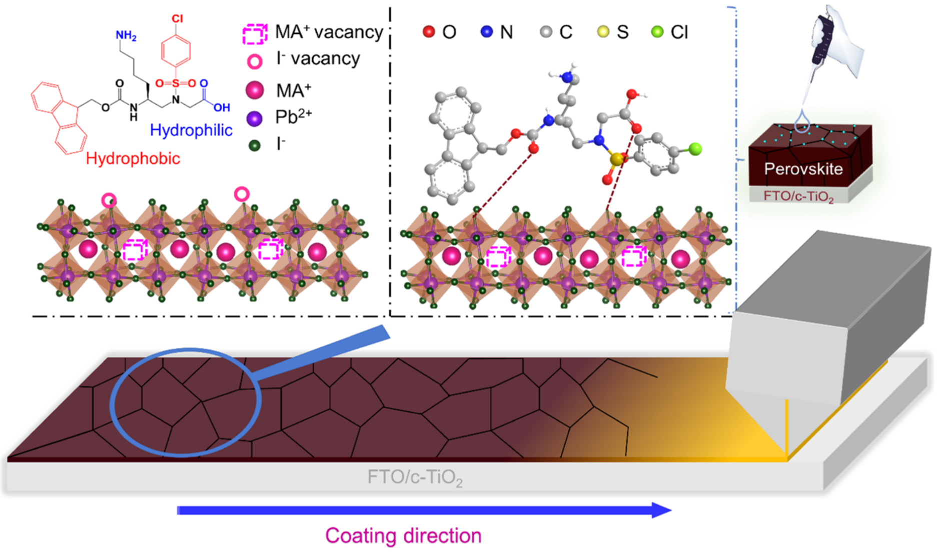

chemical bath deposition (CBD). To understand the sole influence of the F-LYS-S on the perovskite film, we spin-coated various concentrations of it on the surface of the slot-die-coated perovskite layer. The interaction between perovskite and F-LYS-S was systematically investigated with various techniques, including Fourier transform infrared (FTIR) spectroscopy, 2D grazing incidence wide-angle absorption X-ray spectroscopy (2D-GIWAXS) and X-ray photoelectron spectroscopy (XPS). The lone pair electrons of −COOH, −C═O and −NH_2 of the F-LYS-S coordinated with the uncoordinated Pb^{2+} through Lewis acid−base interaction and strengthened the Pb−I bond and blocked the formation of halide vacancies; as a result, the I^- vacancies were repressed effectively.[50] Additionally, the −NH formed strong hydrogen bonding with the perovskite $[PbX_6]^{4-}$ framework to further passivate the halide defects.[51−53] The additional −COOH, −C═O, and −NH_2 in the F-LYS-S strengthened the hydrogen bonding compared with the previously reported amino-acid passivated molecules. Such multiple interactions are verified with FTIR; as a result, F-LYS-S significantly passivated the halide vacancies and considerably lowered trap densities.

Moreover, the F-LYS-S considerably suppressed non-radiative recombination, and the devices demonstrated remarkable charge recombination resistance (tripled that of the control cell); as a result, the F-LYS-S passivated-based device demonstrated substantial improvement in the V_{oc} and FF and produced a champion PCE of 21.08%. Furthermore, the F-LYS-S-modified device displayed excellent moisture stability and maintained 89.6% of its original PCE after 720 h in air (50−60% RH). This study will open a new avenue to realize highly efficient roll-to-roll PSC fabrication at room temperature in air.

EXPERIMENTAL SECTION

Materials. The FTO substrate, all the solvents, and all the chemicals used in this study were purchased from the same supplier mentioned in our previous report.[11] The F-LYS-S passivation molecules were designed and synthesized by our lab.

Device Fabrication. The FTO substrate cleaning procedure was adopted from the literature.[9] The c-TiO_2 was prepared by the water bath technique, following the literature.[11] $MAPbI_3$ slot-die ink was prepared by mixing perovskite gel and acetonitrile (ACN) (1:1 v/v) following the previous report.[11] The perovskite gel preparation is summarized below. Initially, in a 2.56 g MAI vial, 56 mL of ACN was added and stirred at maximum stirring speed. Note that MAI is not dissolved by ACN. Subsequently, 7.38 g of PbI_2 was added, and stirred continuously for 2 h. Then, the black perovskite powder was collected by centrifugation at 6000 rpm for 5 min and dried in a vacuum oven at 70 °C for 2 h.[11] The perovskite powder (3 g) in an open vial and 10 mL of methylamine gas in another open vial were kept together in a closed 100 mL glass container for 4 h to form the perovskite gel.[11]

Next, the perovskite ink was formulated and slot-die-coated on large-area c-TiO_2 at a flow rate of 2.28 $\mu L\ s^{-1}$, a coating speed of 1.2 mm s^{-1}, and a coating gap of 100 μm at 24−25 °C and 30% RH. Afterward, the wet film was annealed at 100 °C for 10 min.

Subsequently, the perovskite film was treated with 2 mM F-LYS-S in 2-propanol. The passivation was employed on 1.5 × 1.5 cm^{-2} area cell, which was cut from the large-area slot-die prepared perovskite film. The passivation molecule was spun at 4000 rpm for 30 s, followed by low-temperature baking (70 °C for 10 min).[11] To complete the device, spiro-OMeTAD and Au (80 nm) were sequentially prepared following the literature.[17]

Characterizations. The interaction between F-LYS-S and the perovskite layer was investigated with FTIR and XPS. The structure/phase of slot-die-coated perovskite were studied in detail by X-ray diffraction (XRD) and 2D-GIWAXS. The morphology of the perovskite layers was studied by scanning electron microscopy (SEM). The optoelectrical properties of the films were investigated by UV−vis, photoluminescence (PL), and time-resolved PL (TRPL). The device *I*−*V*, external quantum efficiency (EQE), and electrochemical impedance spectroscopy (EIS) instruments and measurement conditions were adopted from refs 11 and 17.

RESULTS AND DISCUSSION

Scheme 1 illustrates the fabrication of large-area (10 × 10 cm^2) $MAPbI_3$ perovskite by a slot-die coater on large-area c-TiO_2. The c-TiO_2 was prepared by CBD following our previous report.[11] The digital photograph of the large-area (10 × 10 cm^2) slot-die-coated perovskite is presented in Figure S1. The detailed large-area perovskite layer preparation by the slot-die coater is given in Experimental Section. Subsequently, various concentrations of F-LYS-S in 2-propanol were spun to modify the defects of slot-die prepared $MAPbI_3$. The slot-die coating,

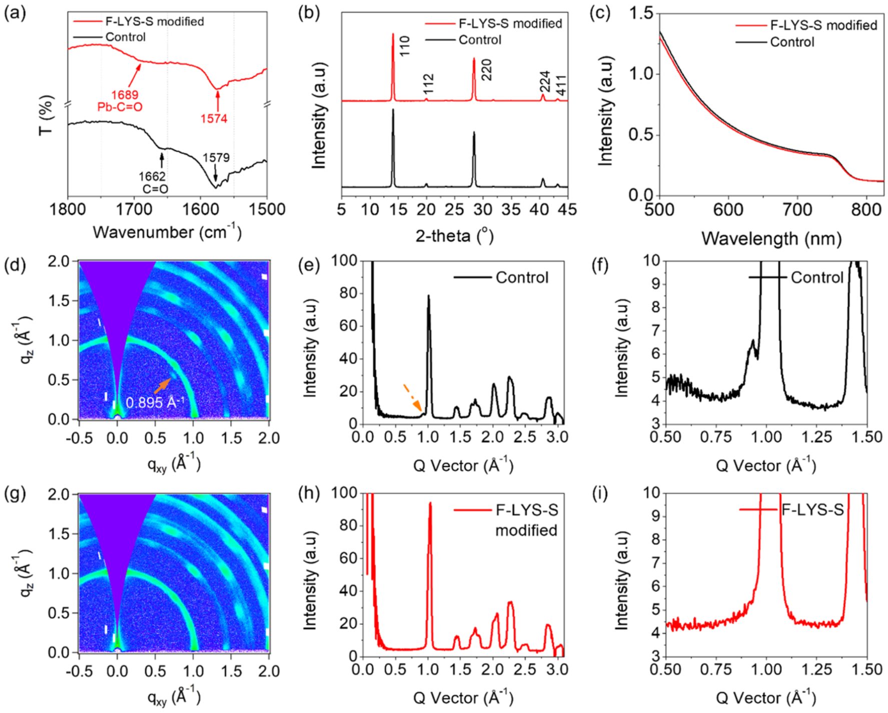

Figure 1. Investigation of the interaction between F-LYS-S and perovskite. (a) Control and F-LYS-S treated perovskite FTIR spectra, (b) control and F-LYS-S treated perovskite XRD, (c) UV−vis of the control and F-LYS-S passivated $MAPbI_3$, (d−f) control $MAPbI_3$ 2D-GIWAXS and its azimuthally integrated intensity profile, respectively. The small spot indicated by the light orange arrow (d) corresponding to 0.895 $Å^{-1}$ (e,f) displayed uncoordinated Pb^{2+} in the standard $MAPbI_3$. (g−i) F-LYS-S-modified $MAPbI_3$ 2D-GIWAXS and its corresponding azimuthally integrated intensity profile, respectively.

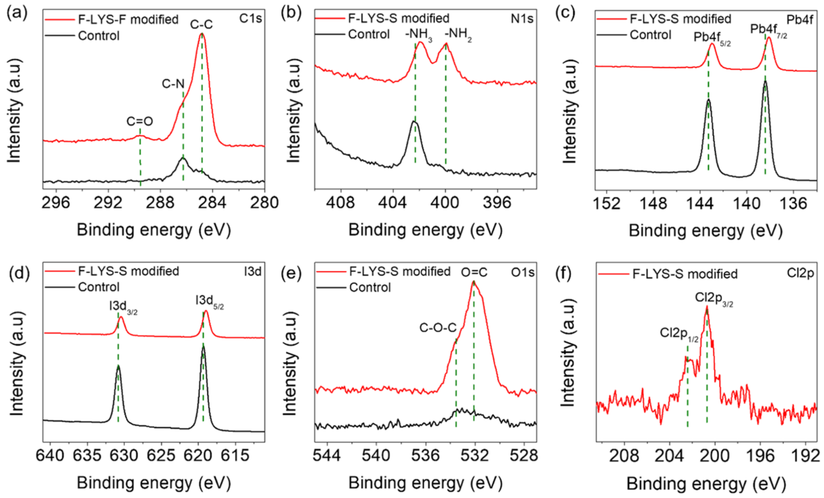

Figure 2. High-resolution XPS peaks of the standard and F-LYS-S passivated perovskite layers. (a) C 1s, (b) N 1s, (c) Pb 4f, (d) I 3d, (e) O 1s, and (f) Cl 2p.

F-LYS-S molecular structure, post-surface modification by spin-coating, and passivation mechanisms are demonstrated in Scheme 1. Following, the coordination of F-LYS-S with $MAPbI_3$ systematically scrutinized with FTIR, 2D-GIWAXS, and XPS.

FTIR spectroscopy was used to investigate the coordination of F-LYS-S with perovskite (Figures 1a and S2a). For comparison, the F-LYS-S powder FTIR is provided in Figure S2b. The FTIR at 1662 cm^{-1} in the control sample assigned to the C═O is significantly shifted to 1689 cm^{-1} for the F-LYS-S-modified perovskite, which indicates the strong interaction between uncoordinated Pb^{2+} ions and the carbonyl group of the F-LYS-S through the Lewis acid−base interaction. Moreover, the N−H stretching vibration (control perovskite = 1579 cm^{-1}) shifted to 1574 cm^{-1} for the F-LYS-S-modified perovskite, which indicated the lone pair containing $-NH_2$ in the F-LYS-S could further interact with the uncoordinated Pb^{2+} ions to suppress I^- defects from the $MAPbI_3$.[17,54] Subsequently, we studied the crystal orientation and phase of the slot-die-coated standard and F-LYS-S-modified $MAPbI_3$, where both films exhibited extremely preferentially oriented sharp peaks at (110), (220), and (224) without any remnant PbI_2 (Figure 1b). The UV−vis characterization (Figure 1c) demonstrated the modification did not influence the

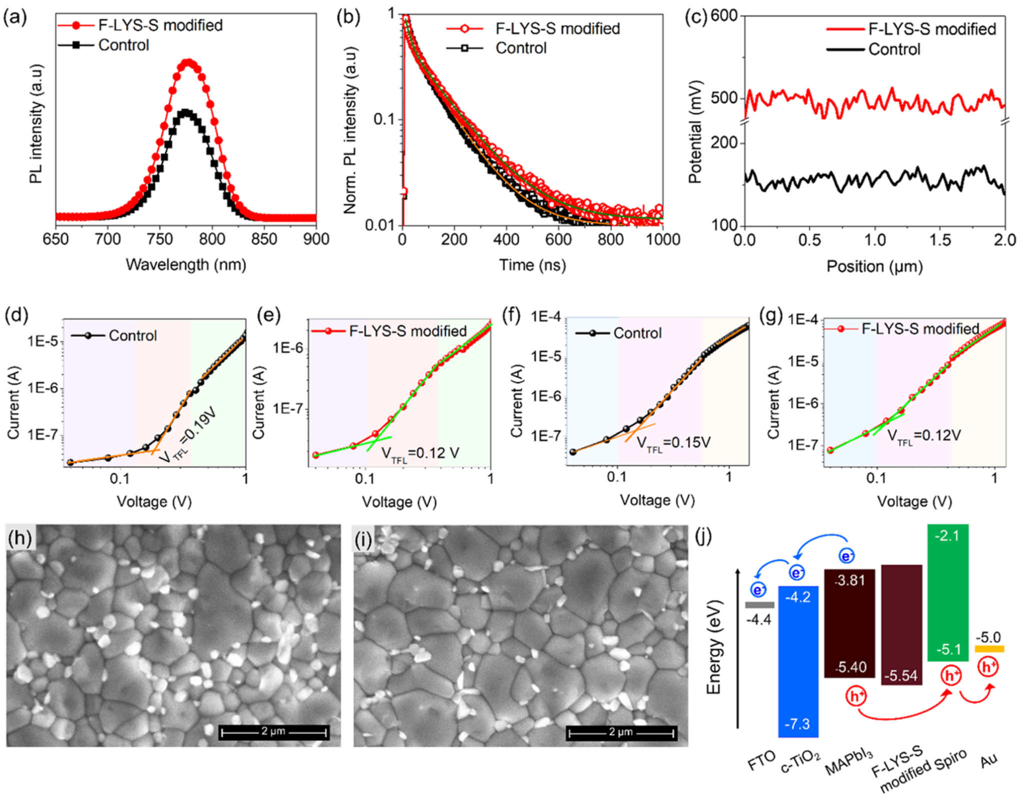

Figure 3. (a) Steady-state PL slot-die-coated perovskite/glass with and without F-LYS-S treatment. (b) TRPL of the standard and F-LYS-S treated perovskite. (c) KPFM contact potential difference of the pristine and F-LYS-S-modified $MAPbI_3$. (d,e) *J*−*V* curves of the electron-only device in the dark [device architectures: FTO/c-TiO_2/perovskite (with/without F-LYS-S)/PCBM/Au]. (f,g) *J*−*V* curves of the hole-only device in the dark [device architectures: FTO/PEDOT:PSS/perovskite (with/without F-LYS-S)/spiro-OMeTAD/Au]. (h) SEM of the bare perovskite. (i) SEM of the F-LYS-S-modified perovskite. (j) Energy level diagram of the F-LYS-S-modified perovskite device.

absorption, which implies that a very thin F-LYS-S layer formed on the perovskite; moreover, the absorption onset of the standard and F-LYS-S-modified perovskite is the same, which suggests that the post-surface modification did not alter the energy level/bandgap of the modified film. To understand the structural orientation details of the control and F-LYS-S-modified perovskite, we measure 2D-GIWAXS. Figure 1d−f and g−i exhibited the GIWAXS and azimuthally integrated intensity of the control and F-LYS-S-modified target perovskite, respectively. Both the control and F-LYS-S-modified perovskite exhibited diffraction rings at 1, 1.4, 1.73, 2, 2.23, 2.45, 2.83, and 3 $Å^{-1}$ corresponding to a 2θ of 14.1, 19.83, 24.48, 28.36, 31.76, 35, 40.55, and 43.18°, respectively. However, we detected a bright spot at 0.895 $Å^{-1}$ (light orange arrow in Figure 1d) in the control perovskite film, which indicates the presence of well-aligned but uncoordinated Pb^{2+} in the control perovskite (Figure 1e−f), which clearly revealed there is an I^- vacancies in the control slot-die-coated perovskite film. The I^- vacancies generated from the post-annealing process and influence the thermodynamic stability of the perovskite and PCE of the devices. Interestingly, the bright Pb^{2+} spot and its associated peak were completely suppressed for the F-LYS-S-modified perovskite (Figure 1h−i), which infers the clear interaction between the F-LYS-S and uncoordinated Pb^{2+} ions, which is consistent with the FTIR result, which leads to reduced I^- vacancy defects. Moreover, both the control and modified perovskite 2D-GIWAXS rings are bright and sharp, which indicates the formation of large grain perovskite, and the strong bright spatter on the ring implies the formation of a well-defined oriented perovskite layer. Large perovskite grain-based perovskite solar devices are known to provide high current density.

We employed high-resolution XPS to get more insight about the interaction between F-LYS-S and perovskite. We measured the C 1s, Pb 4f, O 1s, N 1s, I 3d, Cl 2p, and S 2p XPS spectra of the control and F-LYS-S-modified $MAPbI_3$ films (Figures 2a−f and S3a,b), where we traced the chemical composition changes and distinguished the interaction between F-LYS-S and perovskite based on the binding energy shifts. The C−C peak at 284.84 eV is used to calibrate the XPS peaks.[55] The C 1s spectra are presented in Figure 2a. The modified perovskite exhibited an increase in the C/Pb ratio compared the control perovskite because of the F-LYS-S contains many benzene rings, carbonyls, and carboxyl groups, validating the presence of F-LYS-S on the perovskite surface. The peak at 286.44 eV in the bare $MAPbI_3$ is assigned to C−N, which is shifted to 286.26 eV for the F-LYS-S passivated $MAPbI_3$.[11,56] Furthermore, an additional peak at 289.59 eV was found for the modified perovskite, which is assigned to C═O, which unambiguously validated the interaction between F-LYS-S and the perovskite.[11,57]

Figure 2b shows the N 1s spectra, where a single peak at 402.30 eV (Figure 2b) in the control perovskite is observed, which is assigned to $-NH_3$ that arises from the $MAPbI_3$. Upon F-LYS-S treatment, the $-NH_3$ peak shifted to a lower binding energy of 401.95 eV $MAPbI_3$,[55] which implies the interaction between F-LYS-S and perovskite.[11] Intriguingly, in the N 1s spectra of the F-LYS-S-modified perovskite, an additional peak

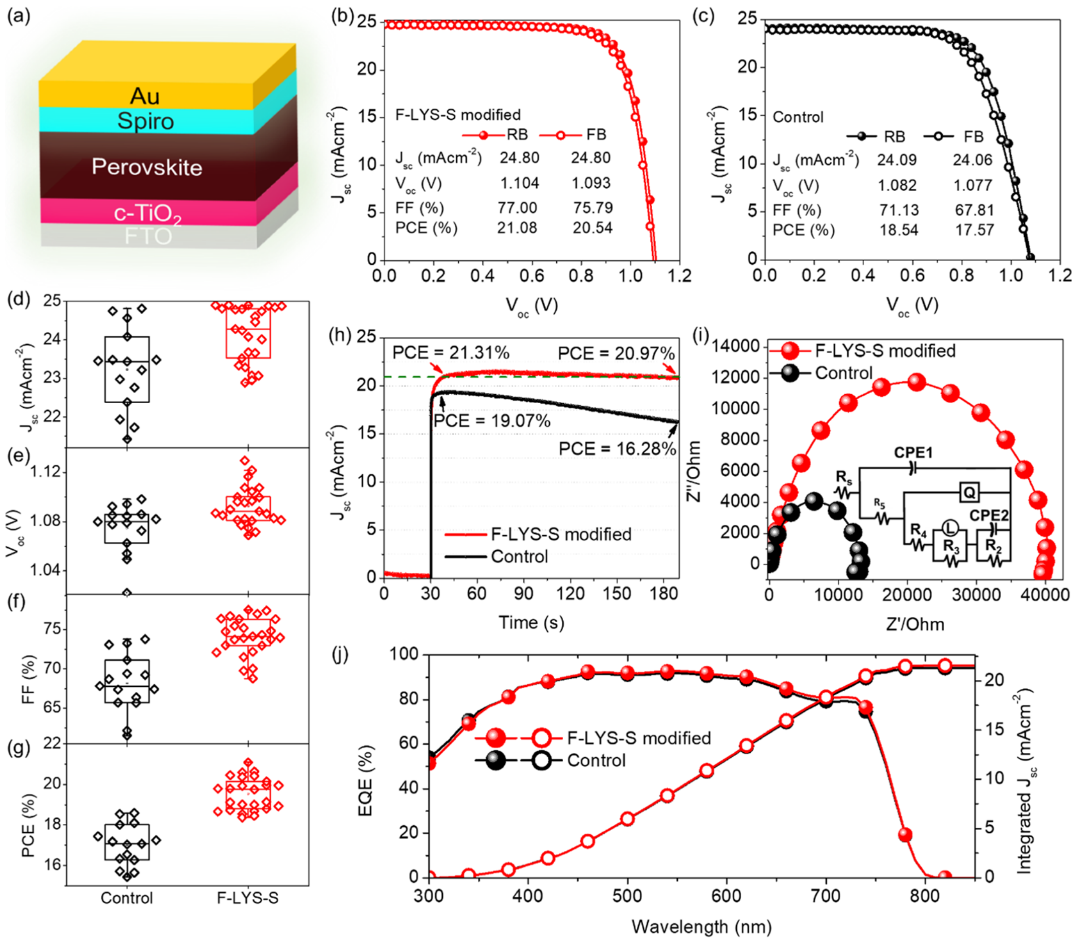

Figure 4. (a) Schematic illustration of PSCs. (b) The champion reverse bias (RB) and forward bias (FB) *I*−*V* curves of the F-LYS-S-modified device. (c) Champion RB and FB *I*−*V* curves of the pristine PSC. Box chart summary of the pristine and F-LYS-S-treated PSCs (d) J_{sc}, (e) V_{oc}, (f) FF, and (g) PCE. (h) Stabilized power output of the control device (at MPP = 0.77 V) and F-LYS-S-treated perovskite (at MPP = 0.85 V). (i) Nyquist plots of the pristine and F-LYS-S-modified $MAPbI_3$-based devices. (j) EQE of the control and F-LYS-S-treated cells.

at 399.94 eV was recorded, which is assigned to $-NH_2$ that originated from the F-LYS-S. The lone pair of $-NH_2$ could coordinate with the uncoordinated Pb^{2+} in the pristine perovskite.[54] These results clearly indicated the interaction between F-LYS-S and perovskite.

Two Pb 4f XPS peaks at 143.27 and 138.43 eV were detected for the standard perovskite, which are assigned to Pb $4f_{5/2}$ and Pb $4f_{7/2}$, respectively (Figure 2c). These peaks are shifted to lower binding energies of 143.01 and 138.13 eV, respectively, for the F-LYS-S treated $MAPbI_3$, suggesting the successful coordination of Pb−N/O/C═O.[11,34] Figure 2d showed the I 3d spectra of the control and F-LYS-S-modified $MAPbI_3$, where the peak at 630.85 eV assigned to I $3d_{3/2}$ and the peak at 619.34 eV assigned to I $3d_{5/2}$ in the pristine perovskite were shifted to lower binding energies of 630.43 and 618.97 eV, respectively, for the F-LYS-S passivated slot-die-coated perovskite layer.[11] Two O 1s peaks were detected for both the standard and modified films at 532.46 and 533.54 eV, which are assigned to O═C and C−O−C, respectively.[58] Like the C/Pb ratio in the O 1s spectra, the O/Pb ratio of the F-LYS-S passivated $MAPbI_3$ perovskite exhibited substantial enhancement compared to the control perovskite because of the extra O from the carboxyl (COOH) and carbonyl (C═O) groups of the F-LYS-S, which further evidenced the perovskite surface was passivated with F-LYS-S (Figure 2e).[11,59]

Additionally, the F-LYS-S-modified perovskite exhibited additional peaks of Cl 2p (Figure 2f) and S 2p (Figure S3b), which are not present in the standard perovskite and undoubtedly deduce the successful surface treatment of $MAPbI_3$ with the F-LYS-S.[11] All the binding energy shifts in the XPS investigation, together with the FTIR and 2D-GIWAXS findings, clearly confirmed the interaction between F-LYS-S and perovskite.

Subsequently, we evaluated the optoelectrical properties of the standard and F-LYS-S-treated perovskite layers to investigate the passivation potential of F-LYS-S. Next, the charge extraction of the standard and F-LYS-S-modified perovskite films was studied by steady-state PL and TRPL on glass/perovskite (with and without F-LYS-S). The excitation light is guided from the perovskite side. However, both the control and modified perovskite exhibited an emission peak at 775 nm, and the PL intensity of the F-LYS-S-modified perovskite was significantly enhanced (∼46%) compared to the pristine $MAPbI_3$ perovskite, which implies that non-radiative recombination is considerably stifled by the F-LYS-S modification, which is a prerequisite to the fabricate high PCE device (Figure 3a).[17,60] In addition, the F-LYS-S-modified film exhibited a prolonged average carrier life time (53.17 ns) compared to the pristine perovskite (44.42 ns), which signified the potential of F-LYS-S to passivate defects (Figure 3b). The average carrier lifetime (τ_{ave}) was calculated using eqs 1 and 2, and the TRPL lifetimes are summarized in Table S1.

$$Y = A_1 \exp\left(\frac{-t}{\tau_1}\right) + A_2 \exp\left(\frac{-t}{\tau_2}\right) \tag{1}$$

$$\tau_{\mathrm{avg}} = \frac{A_1\tau_1^{\,2} + A_2\tau_2^{\,2}}{A_1\tau_1 + A_2\tau_2} \tag{2}$$

Figure 3c showed the contact potential difference (CPD) of the standard and F-LYS-S-modified perovskite measured by Kelvin probe force microscopy (KPFM), where the CPD of the modified perovskite demonstrated more than three-fold enhancement compared to the pristine perovskite (*ca.* 150 *vs* *ca.* 500 mV), which suggested there is a higher potential for charge carrier transport in the passivated film than the standard device, and enhancement in V_{oc} is expected in the modified devices. The V_{oc} of the perovskite devices was influenced by defects.

To quantify the number of electron and hole defects on the standard and F-LYS-S-modified devices, we fabricated electron-only and hole-only devices, respectively. The electron-only devices with the architecture of FTO/c-TiO_2/$MAPbI_3$ (with/without F-LYS-S)/PCBM/Au were fabricated following a literature report to quantify electron traps.[11,61] The number of traps (N_{traps}) is determined using eq 3. The relative dielectric constant of $MAPbI_3$ was adopted from the literature (ε = 32).[11,62] ε_0 and e are constants that represent vacuum permittivity and elementary charge, respectively. The trap-filled limit voltage (V_{TFL}) of the respective devices was found from the dark I−V curve. L is the perovskite film thickness before and after the F-LYS-S modification.

$$N_{\mathrm{traps}} = \frac{2\varepsilon\varepsilon_0 V_{\mathrm{TFL}}}{eL^2} \tag{3}$$

The double logarithmic I−V curves of the pristine and F-LYS-S-treated electron-only cells are shown in Figure 3e,f, where the N_{traps} for the F-LYS-S-modified perovskite significantly reduced by ∼58% from 3.47×10^{15} to 2.19×10^{15} cm^{-3}, which clearly confirmed the potential of F-LYS-S to passivate electron defects. Similarly, the hole-only device, with an architecture of FTO/PEDOT:PSS/perovskite (with/without F-LYS-S)/spiro-OMeTAD/Au (Figure 3g,h) were fabricated to quantify the number of hole traps in the respective devices.[11] The number of hole traps in the control hole-only device was 3.05×10^{15} cm^{-3} and suppressed by ∼25% to 2.44×10^{15} cm^{-3} for the F-LYS-S-treated cell. The number of electron and hole trap studies demonstrated that both electron and hole defects are substantially passivated with the F-LY-S treatment. All the FTIR, 2D-GIWAXS, and XPS already confirmed the interaction of F-LYS-S with perovskite through Lewis acid−base coordination; as a result, the uncoordinated Pb^{2+} ions treated and I^- vacancies significantly suppressed, which is corroborated with the effective repression of electron and hole N_{traps}. The non-radiative recombination in the modified perovskite is significantly reduced; as a result, V_{oc} and FF enhancement in the modified device are expected. The N_{traps} result is coherent with the PL and TRPL investigations. A summary table of SCLC results is provided in Table S2.

The slot-die-coated perovskite produced a compact morphology (Figure 3h). More homogeneous and compact morphology was observed after the F-LYS-S treatment (Figure 3i). The energy level alignment of the pristine and F-LYS-S-treated $MAPbI_3$ film is presented in Figure 3j, where the modified perovskite exhibited a higher work function than the pristine perovskite, which could lead to better charge extraction. As a result, nonradiative recombination could be suppressed in the passivated perovskite.[11,63]

To assess the potential of F-LYS-S on device performance and stability, a planar PSCs with the architecture of FTO/c-TiO_2/perovskite (with/without F-LYS-S)/spiro-OMeTAD/Au was fabricated (Figure 4a). The PSC fabrication is briefly expressed in the Experimental Section. First, we fabricated PSCs with various F-LYS-S concentrations (0, 0.5, 1, 2, and 3 mM) to optimize the best passivation concentration for the $MAPbI_3$ film. The full concentration optimization is provided in Figure S4. At low F-LYS-S concentrations, all the photovoltaic parameters showed typical values, and the PCE improved when the concentration was increased to 1 mM. The best J_{sc}, V_{oc}, and FF were achieved when a 2 mM F-LYS-S concentration was employed. However, when the concentration further increased to 3 mM, the device's performance deteriorated. The optimized 2 mM F-LYS-S-modified perovskite device (Figure 4b) produced remarkable photovoltaic parameters of 1.104 V V_{oc}, 24.80 mA cm^{-2} J_{sc}, and 77% FF with the overall champion efficiency of 21.08% PCE, which is one of the best performances among amino acid-based modified perovskite layers (Table S3). Moreover, our PCE is one of the best among passivated slot-die-coated-based PSCs (Table S4). Furthermore, it also exhibited competitive performance with spin-coated based devices (Table S5). The pristine device displayed the highest PCE of 18.54% with 1.082 V V_{oc}, 24.09 mA cm^{-2} J_{sc}, and 71.13% FF (Figure 4c). The improvement in FF and V_{oc} in the modified device clearly suggested that the F-LYS-S treatment substantially suppressed defects, which is consistent with the PL, TRPL, KPFM, and N_{traps} investigation. The hysteresis index (HI) of the pristine and modified devices was calculated following HI = $(\mathrm{PCE}_{\mathrm{RB}} - \mathrm{PCE}_{\mathrm{FB}})/\mathrm{PCE}_{\mathrm{RB}}$.[17] The control device exhibited an HI of 0.052. Interestingly, the HI of the F-LYS-S-modified device reduced to 0.026, which implied that the modification could suppress surface/bulk defects and interstitial ion migration, which are among the causes of device hysteresis.[64,65] To check the reproducibility of the results, we fabricated 15 control device and 25 F-LYS-S-modified devices, where it is clear that the modified device performance parameters enhanced considerably (Figure 4d−g). Furthermore, achieving uniform and compact perovskite over a large area is necessary for the promising, efficient, and scalable coating process. Considering this, we fabricated a large-area 10 × 10 cm^2 perovskite film using our slot die coating protocol. To investigate the uniformity of the perovskite layer, we measured the UV−vis of the perovskite film in 16 marked places, as seen in Figure S5a. The UV−vis spectra of those perovskite films overlapped each other (Figure S5b), which clearly indicated that uniform perovskite film was formed. Moreover, we fabricated those 16 films after F-LYS-S modification in one batch (Au deposition) process to maintain that every device fabrication step passess through the same fabrication process. The coating area *vs* PCE (%) of those 16 devices is summarized in Figure S5c,d. The fabricated devices demonstrated narrow PCE distribution (20.01 ± 0.58), which suggested a uniform large-area perovskite film was achieved. The F-LYS-S formed strong Lewis acid−base coordination with the perovskite (Pb−C=O/N/O); therefore, the uncoordinated Pb^{2+} ions were

https://doi.org/10.1021/acsami.3c02571

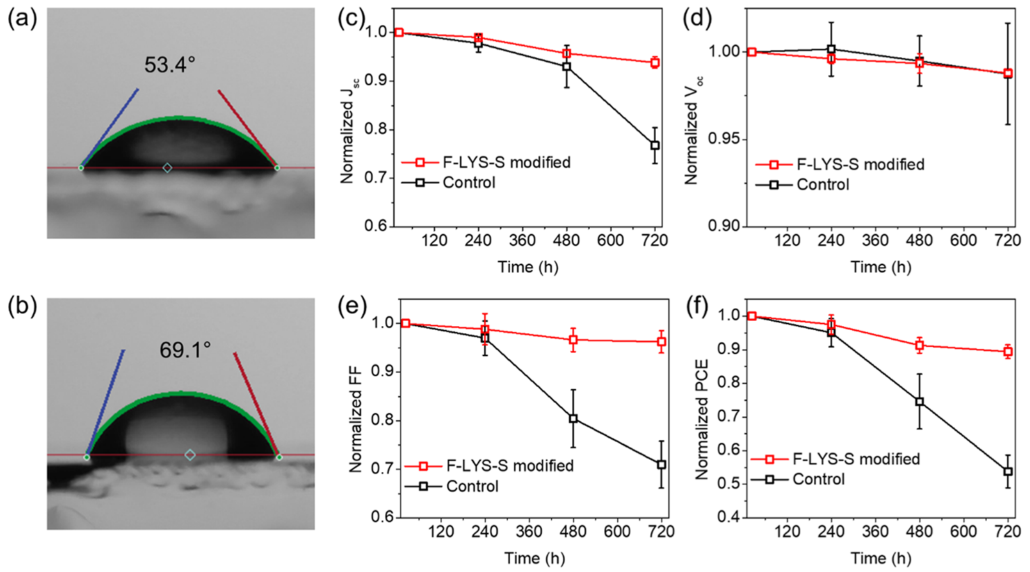

Figure 5. (a) Water contact angle of pristine $MAPbI_3$ and (b) water contact angle of modified $MAPbI_3$. Long-term stability study of the pristine and modified PSCs. Both the control and modified perovskite devices were stored in air at $T \sim 27$ °C and RH = 50−60%, and their photovoltaic parameters were tracked for 720 h. (c) J_{sc}, (d) V_{oc}, (e) FF, and (f) PCE.

substantially repressed, which leads to improvement in V_{oc} and FF. Moreover, the F-LYS-S could form hydrogen bonding with the perovskite by the chloro group of the F-LYS-S (N−H···Cl); as a result, the I^- vacancy was directly repaired with the Cl^-; consecutively, the non-radiative recombination of the modified perovskite was repressed further. The PL of the passivated perovskite demonstrated significant enhancement in photoluminescence that clearly revealed the defects of the pristine perovskite, which were repressed considerably, leading to enhancement of V_{oc} and FF in the modified device. Figure 4h showed the stabilized PCE of the pristine and F-LYS-S treated devices measured at their maximum power point (MPP), where the pristine device performance decreased drastically ~12% from 18.54% PCE to 16.28% PCE in 190 s. Intriguingly, the F-LYS-S-modified device exhibited remarkable stabilized PCE where it maintained its original performance for the same duration of time, which signifies that F-LYS-S not only improved the cell efficiency but also considerably improved the PSC stability.

The charge dynamics process in PSCs is a crucial phenomenon and influences the charge transport and recombination processes; consequently, we scrutinized the charge recombination properties of the pristine and F-LYS-S treated cells by EIS. The $I-V$ curve of the EIS measurement was recorded at 0.9 V bias at dark conditions (Figure 4i). The inset shows their equivalent circuit. The semi-circle at the high frequency of the Nyquist plot is attributed to the charge recombination resistance and geometrical capacitance.[11,66,67] The fitting results are summarized in Table S6. The pristine device series resistance (R_s) is 32.63 Ω, which is decreased to 28.86 Ω for the F-LYS-S-modified device, which is consistent with the FF enhancement for the modified device. Furthermore, the charge recombination resistance (R_2) of the modified devices significantly improved (three-fold) compared to the pristine device (4826 *vs* 1332 Ω), which indisputably verified that the perovskite defects were effectively suppressed by F-LYS-S passivation; thus, the photovoltaic parameters were improved.

The EQE of the pristine and F-LYS-S passivated solar cells produced an integrated J_{sc} of 21.32 and 21.56 mA cm^{-2}, respectively (Figure 4j). The inconsistency in the current densities between the $I-V$ and EQE measurements is in the latter characterization; the J_{sc} measurement was performed at a single wavelength with significantly lower intensity than the one sun radiation.[11,62] In general, the integrated J_{sc} with the discrepancy within the 20% range of the $I-V$ curve J_{sc} suggested a reasonable correlation and reliability.[11,68]

Defects not only reduce the performance of the device but also triggered device instability.[16,69] As a result, we study the stability of the pristine and F-LYS-S films and device. The water contact angle of the pristine $MAPbI_3$ layer is 53.4° (Figure 5a). Upon F-LYS-S modification, the contact angel increased to 69.1° (Figure 5b), which implies the modified film could hamper the infiltration of moisture compared to the pristine perovskite layer.[11] To study the influence of F-LYS-S modification on the long-term stability of the device, four devices each from the control and F-LYS-S-modified were studied to establish a fair and profound stability trend. The pristine device J_{sc}, FF, and PCE rapidly declined (Figure 5c−f) due to severe deterioration with moisture and only maintained 54.4% of their initial performance after a month. Remarkably, the F-LYS-S-modified devices showed notable stability in air and preserved ~89.6% of their initial performance after 720 h.

■ CONCLUSIONS

In summary, we have successfully developed a multi-functional artificial amino acid-sulfonyl-γ-AApeptide-based passivation molecule to effectively modify the defects of slot-die-coated perovskite films. It was found that the F-LYS-S passivation molecule interacted with the $MAPbI_3$ through multiple Lewis acid−base coordination (Pb−C=O/−NH_2/−O) and hydrogen bonding (N−H···Cl) to modify the uncoordinated Pb^{2+} ions and to directly replace I^- ions vacancy, respectively. Consequently, I^- vacancy defects were suppressed effectively, which was verified by the PL enhancement and curtailed N_{traps} for the F-LYS-S-modified film/device. Moreover, the charge recombination resistance of the device considerably improved (three fold) when the slot-die-coated perovskite layer was modified with F-LYS-S. The PL, KPFM, and EIS studies undoubtedly demonstrated that the non-radiative recombination of the slot-die-coated $MAPbI_3$ films wa successfully repressed by F-LYS-S post-surface passivation. As a result, the F-LYS-S treated PSCs produced a champion PCE of 21.08%, with 1.104 V V_{oc}, 24.80 mA cm^{-2} J_{sc}, and 77.00% FF, which is one of the highest results among the reported slot-die-coated PSCs. Furthermore, the modified device exhibited superb long-term stability in air (T = 27 °C and 50−60% RH), where it retained ~89.6% of its initial performance after 720 h.

ASSOCIATED CONTENT

Supporting Information

The Supporting Information is available free of charge at https://pubs.acs.org/doi/10.1021/acsami.3c02571.

Extended FTIR and XPS spectra, TRPL and EIS data, box charts, and a summary of recent slot-die and amino acid-based reports (PDF)

AUTHOR INFORMATION

Corresponding Authors

Jianfeng Cai − *Department of Chemistry, University of South Florida, Tampa, Florida 33620, United States;* orcid.org/0000-0003-3106-3306; Email: jianfengcai@usf.edu

Qilin Dai − *Department of Chemistry, Physics, and Atmospheric Sciences, Jackson State University, Jackson, Mississippi 39217, United States;* orcid.org/0000-0001-8680-4306; Email: qilin.dai@jsums.edu

Authors

Seid Yimer Abate − *Department of Chemistry, Physics, and Atmospheric Sciences, Jackson State University, Jackson, Mississippi 39217, United States*

Ziqi Yang − *Department of Chemistry, University of South Florida, Tampa, Florida 33620, United States*

Surabhi Jha − *School of Polymer Science and Engineering, Center for Optoelectronic Materials and Devices, The University of Southern Mississippi, Hattiesburg, Mississippi 39406, United States*

Jada Emodogo − *Department of Chemistry, Physics, and Atmospheric Sciences, Jackson State University, Jackson, Mississippi 39217, United States*

Guorong Ma − *School of Polymer Science and Engineering, Center for Optoelectronic Materials and Devices, The University of Southern Mississippi, Hattiesburg, Mississippi 39406, United States*

Zhongliang Ouyang − *Department of Electrical and Computer Engineering, Center for Materials for Information Technology, The University of Alabama, Tuscaloosa, Alabama 35487, United States*

Shafi Muhammad − *Department of Chemistry, Physics, and Atmospheric Sciences, Jackson State University, Jackson, Mississippi 39217, United States*

Nihar Pradhan − *Department of Chemistry, Physics, and Atmospheric Sciences, Jackson State University, Jackson, Mississippi 39217, United States;* orcid.org/0000-0002-3912-4233

Xiaodan Gu − *School of Polymer Science and Engineering, Center for Optoelectronic Materials and Devices, The University of Southern Mississippi, Hattiesburg, Mississippi 39406, United States;* orcid.org/0000-0002-1123-3673

Derek Patton − *School of Polymer Science and Engineering, Center for Optoelectronic Materials and Devices, The University of Southern Mississippi, Hattiesburg, Mississippi 39406, United States;* orcid.org/0000-0002-8738-4750

Dawen Li − *Department of Electrical and Computer Engineering, Center for Materials for Information Technology, The University of Alabama, Tuscaloosa, Alabama 35487, United States;* orcid.org/0000-0001-8991-5431

Complete contact information is available at: https://pubs.acs.org/10.1021/acsami.3c02571

Author Contributions

[⊥]S.Y.A. and Z.Y. contributed to the work equally.

Notes

The authors declare no competing financial interest.

ACKNOWLEDGMENTS

This material is based on a work supported by the National Science Foundation (NSF) under grant no. 1757220. The steady-state PL and TRPL equipment used in this work was supported by the National Science Foundation Research Initiation Award: Novel Perovskite Solar Cells Based on Interface Manipulation (award no. 1900047). Q.D. thanks the support of NSF-PREM grant no. DMR-1826886 for the AFM measurements by N.P. XPS instrumentation used in this work was supported by the NSF Major Research Instrumentation Program (DMR-1726901). J.E. was supported by the National Science Foundation under grant no. OIA-2225852. D.L. acknowledges partial support from NSF TIP no. 1919259 for SEM measurements.

REFERENCES

(1) Jeong, J.; Kim, M.; Seo, J.; Lu, H.; Ahlawat, P.; Mishra, A.; Yang, Y.; Hope, M. A.; Eickemeyer, F. T.; Kim, M.; Yoon, Y. J.; Choi, I. W.; Darwich, B. P.; Choi, S. J.; Jo, Y.; Lee, J. H.; Walker, B.; Zakeeruddin, S. M.; Emsley, L.; Rothlisberger, U.; Hagfeldt, A.; Kim, D. S.; Gratzel, M.; Kim, J. Y. Pseudo-Halide Anion Engineering for Alpha-FAPbI3 Perovskite Solar Cells. *Nature* **2021**, *592*, 381−385.

(2) Park, N.-G.; Segawa, H. Research Direction toward Theoretical Efficiency in Perovskite Solar Cells. *ACS Photonics* **2018**, *5*, 2970−2977.

(3) Green, M. A.; Dunlop, E. D.; Hohl-Ebinger, J.; Yoshita, M.; Kopidakis, N.; Bothe, K.; Hinken, D.; Rauer, M.; Hao, X. Solar Cell Efficiency Tables (Version 60). *Prog. Photovolt.: Res. Appl.* **2022**, *30*, 687−701.

(4) Park, N. G. Research Direction toward Scalable, Stable, and High Efficiency Perovskite Solar Cells. *Adv. Energy Mater.* **2019**, *10*, 1903106.

(5) Higuchi, H.; Negami, T. Largest Highly Efficient 203 × 203 mm^2 $CH_3NH_3PbI_3$ Perovskite Solar Modules. *Jpn. J. Appl. Phys.* **2018**, *57*, 08re11.

(6) Lee, D.-K.; Park, N.-G. Materials and Methods for High-Efficiency Perovskite Solar Modules. *Sol. RRL* **2021**, *6*, 2100455.

(7) Kim, H.-J.; Kim, H.-S.; Park, N.-G. Progress of Perovskite Solar Modules. *Adv. Energy Sustainability Res.* **2021**, *2*, 2000051.

(8) Berger, E.; Bagheri, M.; Asgari, S.; Zhou, J.; Kokkonen, M.; Talebi, P.; Luo, J.; Nogueira, A. F.; Watson, T.; Hashmi, S. G. Recent Developments in Perovskite-Based Precursor Inks for Scalable Architectures of Perovskite Solar Cell Technology. *Sustainable Energy Fuels* **2022**, *6*, 2879−2900.

(9) Adugna, G. B.; Abate, S. Y.; Wu, W. T.; Tao, Y. T. Toward Large-Area and Fully Solution-Sheared Perovskite Solar Cells. *ACS Appl. Mater. Interfaces* **2021**, *13*, 25926−25936.

(10) Belay Adugna, G.; Yimer Abate, S.; Tao, Y. T. High-Efficiency and Scalable Solution-Sheared Perovskite Solar Cells using Green Solvents. *Chem. Eng. J.* **2022**, *437*, 135477.

(11) Abate, S. Y.; Yang, Z.; Jha, S.; Ma, G.; Ouyang, Z.; Zhang, H.; Muhammad, S.; Pradhan, N.; Gu, X.; Patton, D.; Wang, K.; Li, D.; Cai, J.; Dai, Q. Room Temperature Slot-Die Coated Perovskite Layer Modified with Sulfonyl-γ-AApeptide for High Performance Perovskite Solar Devices. *Chem. Eng. J.* **2023**, *457*, 141199.

(12) Whitaker, J. B.; Kim, D. H.; Larson, B. W.; Zhang, F.; Berry, J. J.; Van Hest, M. F.; Zhu, K. Scalable Slot-Die Coating of High Performance Perovskite Solar Cells. *Sustainable Energy Fuels* **2018**, *2*, 2442−2449.

(13) Liu, P.; Tang, G.; Yan, F. Strategies for Large-Scale Fabrication of Perovskite Films for Solar Cells. *Sol. RRL* **2021**, *6*, 2100683.

(14) Zimmermann, I.; Al Atem, M.; Fournier, O.; Bernard, S.; Jutteau, S.; Lombez, L.; Rousset, J. Sequentially Slot-Die-Coated Perovskite for Efficient and Scalable Solar Cells. *Adv. Mater. Interfaces* **2021**, *8*, 2100743.

(15) Fievez, M.; Singh Rana, P. J.; Koh, T. M.; Manceau, M.; Lew, J. H.; Jamaludin, N. F.; Ghosh, B.; Bruno, A.; Cros, S.; Berson, S.; Mhaisalkar, S. G.; Leong, W. L. Slot-Die Coated Methylammonium-Free Perovskite Solar Cells with 18% Efficiency. *Sol. Energy Mater. Sol. Cells* **2021**, *230*, 111189.

(16) Byranvand, M. M.; Saliba, M. Defect Passivation of Perovskite Films for Highly Efficient and Stable Solar Cells. *Sol. RRL* **2021**, *5*, 2100295.

(17) Abate, S. Y.; Zhang, Q.; Qi, Y.; Nash, J.; Gollinger, K.; Zhu, X.; Han, F.; Pradhan, N.; Dai, Q. Universal Surface Passivation of Organic-Inorganic Halide Perovskite Films by Tetraoctylammonium Chloride for High-Performance and Stable Perovskite Solar Cells. *ACS Appl. Mater. Interfaces* **2022**, *14*, 28044−28059.

(18) Xiong, J.; Dai, Z.; Zhan, S.; Zhang, X.; Xue, X.; Liu, W.; Zhang, Z.; Huang, Y.; Dai, Q.; Zhang, J. Multifunctional Passivation Strategy Based on Tetraoctylammonium Bromide for Efficient Inverted Perovskite Solar Cells. *Nano Energy* **2021**, *84*, 105882.

(19) Xu, F.; Liu, J.; Subbiah, A. S.; Liu, W.; Kang, J.; Harrison, G. T.; Yang, X.; Isikgor, F. H.; Aydin, E.; De Bastiani, M.; De Wolf, S. Potassium Thiocyanate-Assisted Enhancement of Slot-Die-Coated Perovskite Films for High-Performance Solar Cells. *Small Sci.* **2021**, *1*, 2000044.

(20) Du, M.; Zhu, X.; Wang, L.; Wang, H.; Feng, J.; Jiang, X.; Cao, Y.; Sun, Y.; Duan, L.; Jiao, Y.; Wang, K.; Ren, X.; Yan, Z.; Pang, S.; Liu, S. F. High-Pressure Nitrogen-Extraction and Effective Passivation to Attain Highest Large-Area Perovskite Solar Module Efficiency. *Adv. Mater.* **2020**, *32*, No. e2004979.

(21) Othman, M.; Zheng, F.; Seeber, A.; Chesman, A. S. R.; Scully, A. D.; Ghiggino, K. P.; Gao, M.; Etheridge, J.; Angmo, D. Millimeter-Sized Clusters of Triple Cation Perovskite Enables Highly Efficient and Reproducible Roll-to-Roll Fabricated Inverted Perovskite Solar Cells. *Adv. Funct. Mater.* **2021**, *32*, 2110700.

(22) Jiang, Q.; Zhao, Y.; Zhang, X.; Yang, X.; Chen, Y.; Chu, Z.; Ye, Q.; Li, X.; Yin, Z.; You, J. Surface Passivation of Perovskite Film for Efficient Solar Cells. *Nat. Photonics* **2019**, *13*, 460−466.

(23) De Marco, N.; Zhou, H.; Chen, Q.; Sun, P.; Liu, Z.; Meng, L.; Yao, E. P.; Liu, Y.; Schiffer, A.; Yang, Y. Guanidinium: A Route to Enhanced Carrier Lifetime and Open-Circuit Voltage in Hybrid Perovskite Solar Cells. *Nano Lett.* **2016**, *16*, 1009−1016.

(24) Kim, M.; Kim, G.-H.; Lee, T. K.; Choi, I. W.; Choi, H. W.; Jo, Y.; Yoon, Y. J.; Kim, J. W.; Lee, J.; Huh, D.; Lee, H.; Kwak, S. K.; Kim, J. Y.; Kim, D. S. Methylammonium Chloride Induces Intermediate Phase Stabilization for Efficient Perovskite Solar Cells. *Joule* **2019**, *3*, 2179−2192.

(25) Liu, W.; Xiong, J.; Liu, N.; Dai, J.; Dai, Z.; Huang, Y.; Zhang, Z.; Xue, X.; Dai, Q.; Zhang, J. Defect Passivation and Interface Modification by Tetra-n-octadecyl Ammonium Bromide for Efficient and Stable Inverted Perovskite Solar Cells. *Chem. Eng. J.* **2022**, *429*, 132426.

(26) Shao, Y.; Xiao, Z.; Bi, C.; Yuan, Y.; Huang, J. Origin and Elimination of Photocurrent Hysteresis by Fullerene Passivation in $CH_3NH_3PbI_3$ Planar Heterojunction Solar Cells. *Nat. Commun.* **2014**, *5*, 5784.

(27) Stoddard, R. J.; Rajagopal, A.; Palmer, R. L.; Braly, I. L.; Jen, A. K. Y.; Hillhouse, H. W. Enhancing Defect Tolerance and Phase Stability of High-Bandgap Perovskites via Guanidinium Alloying. *ACS Energy Lett.* **2018**, *3*, 1261−1268.

(28) Zheng, X.; Chen, B.; Dai, J.; Fang, Y.; Bai, Y.; Lin, Y.; Wei, H.; Zeng, X. C.; Huang, J. Defect Passivation in Hybrid Perovskite Solar Cells using Quaternary Ammonium Halide Anions and Cations. *Nat. Energy* **2017**, *2*, 17102.

(29) Zhang, T.; Xie, L.; Chen, L.; Guo, N.; Li, G.; Tian, Z.; Mao, B.; Zhao, Y. In Situ Fabrication of Highly Luminescent Bifunctional Amino Acid Crosslinked 2D/3D $NH_3C_4H_9COO(CH_3NH_3PbBr_3)_n$ Perovskite Films. *Adv. Funct. Mater.* **2017**, *27*, 1603568.

(30) Ye, S.; Rao, H.; Zhao, Z.; Zhang, L.; Bao, H.; Sun, W.; Li, Y.; Gu, F.; Wang, J.; Liu, Z.; Bian, Z.; Huang, C. A Breakthrough Efficiency of 19.9% Obtained in Inverted Perovskite Solar Cells by using an Efficient Trap State Passivator Cu(thiourea)I. *J. Am. Chem. Soc.* **2017**, *139*, 7504−7512.

(31) Choi, K.; Lee, J.; Kim, H. I.; Park, C. W.; Kim, G. W.; Choi, H.; Park, S.; Park, S. A.; Park, T. Thermally Stable, Planar Hybrid Perovskite Solar Cells with High Efficiency. *Energy Environ. Sci.* **2018**, *11*, 3238−3247.

(32) Krishna, A.; Akhavan Kazemi, M. A.; Sliwa, M.; Reddy, G. N. M.; Delevoye, L.; Lafon, O.; Felten, A.; Do, M. T.; Gottis, S.; Sauvage, F. Defect Passivation via the Incorporation of Tetrapropylammonium Cation Leading to Stability Enhancement in Lead Halide Perovskite. *Adv. Funct. Mater.* **2020**, *30*, 1909737.

(33) Kim, J. H.; Kim, Y. R.; Kim, J.; Oh, C. M.; Hwang, I. W.; Kim, J.; Zeiske, S.; Ki, T.; Kwon, S.; Kim, H.; Armin, A.; Suh, H.; Lee, K. Efficient and Stable Perovskite Solar Cells with a High Open-Circuit Voltage Over 1.2 V Achieved by a Dual-Side Passivation Layer. *Adv. Mater.* **2022**, *34*, No. e2205268.

(34) Ji, X.; Feng, K.; Ma, S.; Wang, J.; Liao, Q.; Wang, Z.; Li, B.; Huang, J.; Sun, H.; Wang, K.; Guo, X. Interfacial Passivation Engineering for Highly Efficient Perovskite Solar Cells with a Fill Factor over 83%. *ACS Nano* **2022**, *16*, 11902−11911.

(35) Kim, G. W.; Min, J.; Park, T.; Petrozza, A. Defect Passivation through (alpha-Methylguanido)acetic Acid in Perovskite Solar Cell for High Operational Stability. *ACS Appl. Mater. Interfaces* **2022**, *14*, 20848−20855.

(36) Azmi, R.; Ugur, E.; Seitkhan, A.; Aljamaan, F.; Subbiah, A. S.; Liu, J.; Harrison, G. T.; Nugraha, M. I.; Eswaran, M. K.; Babics, M.; Chen, Y.; Xu, F.; Allen, T. G.; Rehman, A. U.; Wang, C. L.; Anthopoulos, T. D.; Schwingenschlogl, U.; De Bastiani, M.; Aydin, E.; De Wolf, S. Damp Heat-Stable Perovskite Solar Cells with Tailored-Dimensionality 2D/3D Heterojunctions. *Science* **2022**, *376*, 73−77.

(37) Xia, J.; Liang, C.; Mei, S.; Gu, H.; He, B.; Zhang, Z.; Liu, T.; Wang, K.; Wang, S.; Chen, S.; Cai, Y.; Xing, G. Deep Surface Passivation for Efficient and Hydrophobic Perovskite Solar Cells. *J. Mater. Chem. A* **2021**, *9*, 2919−2927.

(38) Lin, C. T.; Xu, W.; Macdonald, T. J.; Ngiam, J.; Kim, J. H.; Du, T.; Xu, S.; Tuladhar, P. S.; Kang, H.; Lee, K.; Durrant, J. R.; McLachlan, M. A. Correlating the Active Layer Structure and Composition with the Device Performance and Lifetime of Amino-Acid-Modified Perovskite Solar Cells. *ACS Appl. Mater. Interfaces* **2021**, *13*, 43505−43515.

(39) Jia, D.; Chen, J.; Yu, M.; Liu, J.; Johansson, E. M. J.; Hagfeldt, A.; Zhang, X. Dual Passivation of $CsPbI_3$ Perovskite Nanocrystals with Amino Acid Ligands for Efficient Quantum Dot Solar Cells. *Small* **2020**, *16*, No. e2001772.

(40) Han, J.; Kim, K.; Nam, J. S.; Hong, S. J.; Choi, E. J.; Kim, D.; Chung, I.; Lin, H. S.; Kim, T. D.; Strano, M. S.; Han, B.; Oh, J. W.; Kim, H. D.; Jeon, I. Genetic Manipulation of M13 Bacteriophage for Enhancing the Efficiency of Virus-Inoculated Perovskite Solar Cells with a Certified Efficiency of 22.3%. *Adv. Energy Mater.* **2021**, *11*, 2101221.

(41) Ma, B.; Sun, X.; Yan, S.; Zhang, L.; Chen, S.; Liu, X.; Song, J. Interface Modification by Fmoc-Met-OH Molecule for High-Efficient

Perovskite Solar Cells. *J. Mater. Sci.: Mater. Electron.* **2022**, *33*, 15359−15368.

(42) Xu, P.; Xie, L.; Yang, S.; Han, B.; Liu, J.; Chen, J.; Liu, C.; Jia, R.; Yang, M.; Ge, Z. Manipulating Halide Perovskite Passivation by Controlling Amino Acid Derivative Isoelectric Point for Stable and Efficient Inverted Perovskite Solar Cells. *Sol. RRL* **2023**, *7*, 2200858.

(43) Rana, P. J. S.; Febriansyah, B.; Koh, T. M.; Muhammad, B. T.; Salim, T.; Hooper, T. J. N.; Kanwat, A.; Ghosh, B.; Kajal, P.; Lew, J. H.; Aw, Y. C.; Yantara, N.; Bruno, A.; Pullarkat, S. A.; Ager, J. W.; Leong, W. L.; Mhaisalkar, S. G.; Mathews, N. Alkali Additives Enable Efficient Large Area (>55 cm^2) Slot-Die Coated Perovskite Solar Modules. *Adv. Funct. Mater.* **2022**, *32*, 2113026.

(44) Benitez-Rodriguez, J. F.; Chen, D.; Scully, A. D.; Easton, C. D.; Vak, D.; Li, H.; Shaw, P. E.; Burn, P. L.; Caruso, R. A.; Gao, M. Slot-Die Coating of a Formamidinium-Cesium Mixed-Cation Perovskite for Roll-to-Roll Fabrication of Perovskite Solar Cells Under Ambient Laboratory Conditions. *Sol. Energy Mater. Sol. Cells* **2022**, *246*, 111884.

(45) Lee, H.-J.; Na, S.-I. Efficient Mixed-Cation Perovskite Photovoltaic Cells via Additive-Assisted Slot-Die Deposition. *Mater. Res. Bull.* **2022**, *149*, 111728.

(46) Bernard, S.; Jutteau, S.; Mejaouri, S.; Cacovich, S.; Zimmermann, I.; Yaiche, A.; Gbegnon, S.; Loisnard, D.; Collin, S.; Duchatelet, A.; Sauvage, F.; Rousset, J. One-Step Slot-Die Coating Deposition of Wide-Bandgap Perovskite Absorber for Highly Efficient Solar Cells. *Sol. RRL* **2021**, *5*, 2100391.

(47) Li, J.; Dagar, J.; Shargaieva, O.; Flatken, M. A.; Köbler, H.; Fenske, M.; Schultz, C.; Stegemann, B.; Just, J.; Többens, D. M.; Abate, A.; Munir, R.; Unger, E. 20.8% Slot-Die Coated $MAPbI_3$ Perovskite Solar Cells by Optimal DMSO-Content and Age of 2-ME Based Precursor Inks. *Adv. Energy Mater.* **2021**, *11*, 2003460.

(48) Yang, Z.; Zhang, W.; Wu, S.; Zhu, H.; Liu, Z.; Liu, Z.; Jiang, Z.; Chen, R.; Zhou, J.; Lu, Q.; Xiao, Z.; et al. Slot-die coating large-area formamidinium-cesium perovskite film for efficient and stable parallel solar module. *Sci. Adv.* **2021**, *7*, No. eabg3749.

(49) Sang, P.; Shi, Y.; Huang, B.; Xue, S.; Odom, T.; Cai, J. Sulfono-γ-AApeptides as Helical Mimetics: Crystal Structures and Applications. *Acc. Chem. Res.* **2020**, *53*, 2425−2442.

(50) Zou, K.; Li, Q.; Fan, J.; Tang, H.; Chen, L.; Tao, S.; Xu, T.; Huang, W. Pyridine Derivatives' Surface Passivation Enables Efficient and Stable Carbon-Based Perovskite Solar Cells. *ACS Mater. Lett.* **2022**, *4*, 1101−1111.

(51) Yun, S.-C.; Ma, S.; Kwon, H.-C.; Kim, K.; Jang, G.; Yang, H.; Moon, J. Amino Acid Salt-Driven Planar Hybrid Perovskite Solar Cells with Enhanced Humidity Stability. *Nano Energy* **2019**, *59*, 481−491.

(52) Yang, S.; Dai, J.; Yu, Z.; Shao, Y.; Zhou, Y.; Xiao, X.; Zeng, X. C.; Huang, J. Tailoring Passivation Molecular Structures for Extremely Small Open-Circuit Voltage Loss in Perovskite Solar Cells. *J. Am. Chem. Soc.* **2019**, *141*, 5781−5787.

(53) Wang, R.; Xue, J.; Wang, K. L.; Wang, Z. K.; Luo, Y.; Fenning, D.; Xu, G.; Nuryyeva, S.; Huang, T.; Zhao, Y.; Yang, J. L.; et al. Constructive Molecular Monfigurations for Surface-Defect Passivation of Perovskite Photovoltaics. *Science* **2019**, *366*, 1509−1513.

(54) Wang, S.; Wang, A.; Deng, X.; Xie, L.; Xiao, A.; Li, C.; Xiang, Y.; Li, T.; Ding, L.; Hao, F. Lewis Acid/Base Approach for Efficacious Defect Passivation in Perovskite Solar Cells. *J. Mater. Chem. A* **2020**, *8*, 12201−12225.

(55) Wang, S.; Cao, F.; Wu, Y.; Zhang, X.; Zou, J.; Lan, Z.; Sun, W.; Wu, J.; Gao, P. Multifunctional 2D Perovskite Capping Layer using Cyclohexylmethylammonium Bromide for Highly Efficient and Stable Perovskite Solar Cells. *Mater. Today Phys.* **2021**, *21*, 100543.

(56) Yang, B.; Suo, J.; Mosconi, E.; Ricciarelli, D.; Tress, W.; De Angelis, F.; Kim, H.-S.; Hagfeldt, A. Outstanding Passivation Effect by a Mixed-Salt Interlayer with Internal Interactions in Perovskite Solar Cells. *ACS Energy Lett.* **2020**, *5*, 3159−3167.

(57) Hu, J.; Xu, X.; Chen, Y.; Wu, S.; Wang, Z.; Wang, Y.; Jiang, X.; Cai, B.; Shi, T.; Brabec, C. J.; Mai, Y.; Guo, F. Overcoming Photovoltage Deficit via Natural Amino Acid Passivation for Efficient Perovskite Solar Cells and Modules. *J. Mater. Chem. A* **2021**, *9*, 5857−5865.

(58) López, G. P.; Castner, D. G.; Ratner, B. D. XPS O 1s Binding Energies for Polymers Containing Hydroxyl, Ether, Ketone and Ester Groups. *Surf. Interface Anal.* **1991**, *17*, 267−272.

(59) Hu, B.; Zhang, J.; Guo, Z.; Lu, L.; Li, P.; Chen, M.; Li, C. Manipulating Ion Migration and Interfacial Carrier Dynamics via Amino Acid Treatment in Planar Perovskite Solar Cells. *ACS Appl. Mater. Interfaces* **2022**, *14*, 15840−15848.

(60) Ma, C.; Park, N.-G. Paradoxical Approach with a Hydrophilic Passivation Layer for Moisture-Stable, 23% Efficient Perovskite Solar Cells. *ACS Energy Lett.* **2020**, *5*, 3268−3275.

(61) Abate, S. Y.; Zhang, Q.; Qi, Y.; Nash, J.; Gollinger, K.; Zhu, X.; Han, F.; Pradhan, N.; Dai, Q. Universal Surface Passivation of Organic-Inorganic Halide Perovskite Films by Tetraoctylammonium Chloride for High-Performance and Stable Perovskite Solar Cells. *ACS Appl. Mater. Interfaces* **2022**, *14*, 28044−28059.

(62) Abate, S. Y.; Wu, W. T.; Pola, S.; Tao, Y. T. Compact TiO_2 Films with Sandwiched Ag Nanoparticles as Electron-Collecting Layer in Planar Type Perovskite Solar Cells: Improvement in Efficiency and Stability. *RSC Adv.* **2018**, *8*, 7847−7854.

(63) Ansari, F.; Shirzadi, E.; Salavati-Niasari, M.; LaGrange, T.; Nonomura, K.; Yum, J. H.; Sivula, K.; Zakeeruddin, S. M.; Nazeeruddin, M. K.; Gratzel, M.; Dyson, P. J.; Hagfeldt, A. Passivation Mechanism Exploiting Surface Dipoles Affords High-Performance Perovskite Solar Cells. *J. Am. Chem. Soc.* **2020**, *142*, 11428−11433.

(64) Singh, A.; Abate, S. Y.; Pavan Kumar, C.; Wu, W.-T.; Hsiao, J.-C.; Wu, F.-L.; Lin, J. T. s.; Tao, Y.-T. Bis(diphenylamine)-Tethered Carbazolyl Anthracene Derivatives as Hole-Transporting Materials for Stable and High-Performance Perovskite Solar Cells. *ACS Appl. Energy Mater.* **2020**, *3*, 10752−10764.

(65) Liu, P.; Wang, W.; Liu, S.; Yang, H.; Shao, Z. Fundamental Understanding of Photocurrent Hysteresis in Perovskite Solar Cells. *Adv. Energy Mater.* **2019**, *9*, 1803017.

(66) Bou, A.; Pockett, A.; Raptis, D.; Watson, T.; Carnie, M. J.; Bisquert, J. Beyond Impedance Spectroscopy of Perovskite Solar Cells: Insights from the Spectral Correlation of the Electrooptical Frequency Techniques. *J. Phys. Chem. Lett.* **2020**, *11*, 8654−8659.

(67) Guerrero, A.; Bisquert, J.; Garcia-Belmonte, G. Impedance Spectroscopy of Metal Halide Perovskite Solar Cells from the Perspective of Equivalent Circuits. *Chem. Rev.* **2021**, *121*, 14430−14484.

(68) Christians, J. A.; Manser, J. S.; Kamat, P. V. Best Practices in Perovskite Solar Cell Efficiency Measurements. Avoiding the Error of Making Bad Cells Look Good. *J. Phys. Chem. Lett.* **2015**, *6*, 852−857.

(69) Kang, D.-H.; Kim, S.-Y.; Lee, J.-W.; Park, N.-G. Efficient Surface Passivation of Perovskite Films by a Post-Treatment Method with a Minimal Dose. *J. Mater. Chem. A* **2021**, *9*, 3441−3450.